ELSEVIER

NeuroImage

www.elsevier.com/locate/ynimg
NeuroImage 31 (2006) 160 – 171

# Assessing and improving the spatial accuracy in MEG source localization by depth-weighted minimum-norm estimates

Fa-Hsuan Lin, [a,*] Thomas Witzel,[a,b] Seppo P. Ahlfors,[a] Steven M. Stufflebeam,[a] John W. Belliveau,[a] and Matti S. Hämäläinen [a]

[a]*MGH/MIT/HMS Athinoula A. Martinos Center for Biomedical Imaging, Building 149 13th St. Charlestown, MA 02129, USA*
[b]*Harvard-MIT Division of Health Sciences and Technology, Massachusetts Institute Technology, 77 Massachusetts Avenue, Cambridge, MA 02139, USA*

Received 16 March 2005; revised 21 November 2005; accepted 29 November 2005
Available online 6 March 2006

**Cerebral currents responsible for the extra-cranially recorded magnetoencephalography (MEG) data can be estimated by applying a suitable source model. A popular choice is the distributed minimum-norm estimate (MNE) which minimizes the $\ell_2$-norm of the estimated current. Under the $\ell_2$-norm constraint, the current estimate is related to the measurements by a linear inverse operator. However, the MNE has a bias towards superficial sources, which can be reduced by applying depth weighting. We studied the effect of depth weighting in MNE using a shift metric. We assessed the localization performance of the depth-weighted MNE as well as depth-weighted noise-normalized MNE solutions under different cortical orientation constraints, source space densities, and signal-to-noise ratios (SNRs) in multiple subjects. We found that MNE with depth weighting parameter between 0.6 and 0.8 showed improved localization accuracy, reducing the mean displacement error from 12 mm to 7 mm. The noise-normalized MNE was insensitive to depth weighting. A similar investigation of EEG data indicated that depth weighting parameter between 2.0 and 5.0 resulted in an improved localization accuracy. The application of depth weighting to auditory and somatosensory experimental data illustrated the beneficial effect of depth weighting on the accuracy of spatiotemporal mapping of neuronal sources.**


*Keywords:* Inverse problem; MEG; Depth; Minimum-norm; Brain

## Introduction

Magnetoencephalography (MEG) records the extra-cranial magnetic field using super-conducting quantum interferences device (SQUID), allowing electrical neural activity to be studied completely non-invasively (Hamalainen et al., 1993). Localization of the sources of MEG signals is complicated by the non-uniqueness of the electromagnetic inverse problem (Helmholtz, 1853). In order to render the solution unique, several source modeling techniques with different constraints have been proposed. In the equivalent current dipole (ECD) approach, the activation is assumed relatively focal, and it can be thus well accounted for by a small number of current dipoles. However, the assumption of limited extent of the activity cannot always be justified. Furthermore, reliable estimation of the non-linear dipole location parameters becomes prohibitively difficult when the number of sources increases. Some of the limitations of the ECD model can be overcome by using a distributed source model. In this approach, the locations of a large number of dipoles are kept fixed, and their amplitudes are determined on the basis of the measured data. This problem is under-determined; therefore, additional a priori constraints are required. In the $\ell_2$ minimum-norm estimate (MNE) approach (Hamalainen and Ilmoniemi, 1984), one selects the current distribution with minimum power ($\ell_2$-norm) while maintaining the requirement that the measured data match those predicted by the model. This MNE solution was subsequently extended to incorporate cortical location and orientation constraints (Dale and Sereno, 1993). Furthermore, noise normalization has been employed to establish the statistical significance of current estimates (Dale et al., 2000). In accordance with similar approaches used in other functional imaging modalities (fMRI and PET), the resulting spatiotemporal estimates are often referred to as dynamic statistical parametric maps, dSPM. Subsequently, a variation of this approach (sLORETA) has been introduced (Pascual-Marqui, 2002).

For the calculation of source estimates, the solution of the forward problem, i.e., the calculation of the signals generated by the dipole sources in the extra-cranial MEG sensor measurements, is a prerequisite. Realistic anatomical information can be incorporated in the forward model by using the Boundary Element Method (BEM) (Hamalainen and Sarvas, 1989; Oostendorp and van Oosterom, 1989). Because MEG signals originate mainly in the cortex, the source locations and orientations can be constrained with help of high-resolution cortical surface reconstructions (Dale et al., 1999; Fischl et al., 1999).

* Corresponding author. Fax: +1 617 726 7422.
*E-mail address:* fhlin@nmr.mgh.harvard.edu (F.-H. Lin).
**Available online on ScienceDirect (www.sciencedirect.com).**

1053-8119/$ – see front matter © 2005 Elsevier Inc. All rights reserved.
doi:10.1016/j.neuroimage.2005.11.054

The sensitivity pattern of a given MEG sensor to intracranial sources is called the lead field, which can be computed in a straightforward manner once an accurate forward model is available. However, the sensitivity of MEG sensors is not uniform to sources across different cortical locations (Hillebrand and Barnes, 2002). In fact, it follows generally from Maxwell's equations that the lead fields of both MEG sensors and EEG electrodes have a maximum at the border of the source space, closest to the sensors (Heller and van Hulsteyn, 1992). The MNE solution is biased to those locations to which the sensors are most sensitive, thus the preference of superficial source locations. In fact, both $\ell_2$ minimum-norm (MNE) and $\ell_1$ minimum-norm (minimum-current estimate, MCE) (Uutela et al., 1999) solutions are biased toward superficial source locations (Uutela et al., 1999). These biases can potentially be alleviated by adjusting assumptions about the a priori source covariance. A norm of the lead field has been employed earlier in depth weighting (Fuchs et al., 1999; Ioannides et al., 1990). However, there are no systematic studies on the effect of depth weighting and selection of optimal weighting for accurate localization of sources.

Here, we report a parametric study in different subjects, dipole orientation constraints, source space densities, and SNR in the measurements to evaluate the biases toward superficial sources in the MEG MNE. We attempt to alleviate this bias with depth weighting and to quantify the amount of bias by introducing source location shift metrics. Subsequently, we look for an optimal depth weighting parameter to minimize the shift metrics. Using realistic brain anatomy from multiple subjects, our analysis shows the impact of depth weighting parameter on the localization accuracy of MNE (including noise-normalized MNE) with different cortical orientation constraints. An optimal depth weighting parameter is suggested, and realistic auditory and somatosensory MEG experiment results are shown to demonstrate the benefits of depth weighting.

## Method

### *Minimum-norm estimate*

The measured MEG/EEG signals and underlying current source strengths are related by a linear transformation:

$$\mathbf{Y} = \mathbf{AX} + \mathbf{N}, \tag{1}$$

where $\mathbf{Y}$ is an $m$-by-$t$ matrix containing measurements from $m$ sensors over $t$ distinct time instants, $\mathbf{X}$ is a $3n$-by-$t$ matrix denoting the unknown time-dependent amplitudes of the three directionally orthogonal components of $n$ current sources, $\mathbf{A}$ is the gain matrix (forward solution). The rows of $\mathbf{A}$ are called lead fields; they represent the mapping from the current elements to the MEG sensors. $\mathbf{N}$ is an $m$-by-$t$ matrix denoting noise in the measured data. Assuming that $\mathbf{X}$ and $\mathbf{N}$ are stationary, Gaussian distributed with zero mean and a spatial covariance matrix $\mathbf{R}$ and $\mathbf{C}$, respectively, the regularized $\ell_2$ minimum-norm estimate of $\mathbf{X}$ is (Tarantola, 1987):

$$\mathbf{X}^{\mathrm{MNE}} = \mathbf{RA}^T\left(\mathbf{ARA}^T + \lambda^2\mathbf{C}\right)^{-1}\mathbf{Y} = \mathbf{W}^{\mathrm{MNE}}\mathbf{Y}, \tag{2}$$

where $\lambda^2$ is a regularization parameter to avoid magnification of errors in data in the current solution, and the superscript $^T$ indicates the matrix transpose.

Instead of applying Eq. (2) directly, it is convenient to use an equivalent formulation

$$\mathbf{X}^{\mathrm{MNE}} = \mathbf{R}\tilde{\mathbf{A}}^T\left(\tilde{\mathbf{A}}\mathbf{R}\tilde{\mathbf{A}}^T + \lambda^2\mathbf{I}\right)^{-1}\tilde{\mathbf{Y}} = \tilde{\mathbf{W}}^{\mathrm{MNE}}\tilde{\mathbf{Y}}, \tag{3}$$

where

$$\tilde{\mathbf{Y}} = \mathbf{C}^{-1/2}\mathbf{Y}$$

$$\tilde{\mathbf{A}} = \mathbf{C}^{-1/2}\mathbf{A} \tag{4}$$

are the spatially whitened data and spatially whitened gain matrix, respectively. The noise-covariance matrix of the whitened data is an identity matrix, as indicated by the comparison between Eqs. (2) and (3). The whitening procedure also allows one to use the scaling $\lambda^2 = \delta^2 tr\ (\tilde{\mathbf{A}}\tilde{\mathbf{R}}\tilde{\mathbf{A}}^T)/m$, where $\delta^2$ denotes the inverse of the power SNR of the whitened data to bring the regularization parameter to a reasonable scale even in cases where the measurements have different units of measure, which is the case when planar gradiometer and magnetometer data or MEG and EEG data are combined in a single estimate.

### *Anatomical constraints and Cortical Patch Statistics (CPS)*

Anatomical information can be taken into account in the model by selecting the source elements to be located on the cortical surface. Furthermore, a priori orientation information can be incorporated (Dale and Sereno, 1993; Fuchs et al., 1999; Phillips et al., 2002; Wang et al., 1992) by replacing Eq. (1) with

$$\mathbf{Y} = \mathbf{A}_{\mathrm{fixed}}\mathbf{X}_{\mathrm{fixed}} + \mathbf{N},$$

where the new gain matrix is

$$\mathbf{A}_{\mathrm{fixed}} = \mathbf{A}\Theta; \tag{5}$$

$\Theta$ is a $3n$-by-$n$ matrix containing the unit vectors pointing to the directions of the currents. If the direction cosines of the $k$th dipole are $c_{\mathrm{kx}}$, $c_{\mathrm{ky}}$, and $c_{\mathrm{kz}}$, the $k$th column of $\Theta$ reads

$$\Theta_k = \left(\underbrace{0\ldots0}_{3(k-1)}\, c_{\mathrm{kx}}c_{\mathrm{ky}}c_{\mathrm{kz}}\, \underbrace{0\ldots0}_{n-3k}\right)^T. \tag{6}$$

In MEG/EEG source modeling, the dense anatomical model tessellation with approximately 1-mm triangle size is typically decimated to a grid spacing of 5–10 mm. This is motivated by the limited spatial resolution intrinsic to the source localization using MEG/EEG and computational efficiency concerns. However, this sparse source spacing may yield inaccurate dipole orientations, which do not take into account the orientation variation over the cortical patch associated with each selected current source location. Furthermore, the actual areas of the patches have to be taken into account in the calculations to correctly estimate the current density on the cortex. Recently, we introduced the use flexible anatomical constraint based on the calculation of Cortical Patch Statistics (CPS) (Lin et al., 2003). This method uses the geometry of the cortical surface segmented from high-resolution 3D MRI. We employ the FreeSurfer software (Dale et al., 1999; Fischl et al., 1999, 2001), which builds the triangular cortical surface mesh from T1-weighted anatomical MRI data with a 1-mm isotropic spatial resolution. The principal surfaces generated by FreeSurfer are the pial surface and the gray–white matter boundary; we use the latter

to generate the cortically constrained source space. After decimating the cortical surface tessellation to the desired source space grid spacing, the cortical patches associated with each source space points are defined. For each patch, we compute the following characteristics: the average normal direction within a patch, the dispersion of normal directions, and the size of the patch. This information is incorporated into the source covariance matrix **R** to improve the anatomical description in MNE.

In our simulations with depth weighting, we employed three orientation constraints: free source orientations (FO), strict orientation constraint (SOC), and loose orientation constraint (LOC) were used separately in the depth weighting calculations. In FO, the amplitudes of the 3 orthogonal directional components for each dipole source are estimated. In SOC, the orientation of the dipole is strictly constrained to be perpendicular to the cortical surface and only one amplitude is estimated at each dipole source. In LOC, we estimate all three orthogonal dipole components with smaller a priori variance for the tangential components compared to the perpendicular one (Lin et al., 2006).

### *Noise-normalized estimates*

Analogously to the statistical parametric maps (SPMs) calculated in other functional imaging modalities, Dale et al. (2000) proposed the conversion of the current values into dynamic SPMs by a normalization with the estimated noise at each source. To this end, we need to consider the variance of the estimated current at location $k$:

$$w_k^2 = \left(\mathbf{WCW}^T\right)_{kk} = \left(\tilde{\mathbf{W}}\tilde{\mathbf{W}}^T\right)_{kk}. \tag{7}$$

For fixed-orientation sources, we now obtain the noise-normalized activity estimate for the $k$th dipole and $t$th time point as

$$z_{kt}^{\mathrm{dSPM}} = \frac{X_{k,t}^{\mathrm{MNE}}}{w_k} \tag{8}$$

which is $t$-distributed under the null hypothesis of no activity at the current location $k$. Since the number of time samples used to calculate the noise-covariance matrix **C** is quite large, more than 100, the $t$ distribution approaches a unit normal distribution (i.e., a $z$ score).

If the orientation is not constrained, the noise-normalized solution is calculated as

$$F_{kt}^{\mathrm{dSPM}} = \frac{\sum_{q=1}^{3}\left(X_{3(k-1)+q,\,t}^{\mathrm{MNE}}\right)^2}{\sum_{q=1}^{3} w_{3(k-1)+q}^2}. \tag{9}$$

Under the null hypothesis, $F_{kp}^{\mathrm{dSPM}}$ is $F$-distributed, with three degrees of freedom for the numerator. The degree of freedom for the denominator is typically large, again depending on the number of time samples used to calculate the noise-covariance matrix.

Another variation of the noise-normalized MNE is the sLORETA (Pascual-Marqui, 2002):

$$\tilde{w}_k^2 = \left(\mathbf{W}\left(\mathbf{C} + \mathbf{ARA}^T\right)\mathbf{W}^T\right)_{kk} = \left(\tilde{\mathbf{W}}\left(\mathbf{I} + \tilde{\mathbf{A}}\mathbf{R}\tilde{\mathbf{A}}^T\right)\tilde{\mathbf{W}}^T\right)_{kk}. \tag{10}$$

### *Depth weighting*

The MNE is known to have a bias towards superficial currents, associated with the attenuation of the MEG and EEG lead fields with increasing source depth. To compensate for this bias, modification of the source-covariance matrix has been previously employed. In this approach, the variances are taken to be proportional to a scaling a function, denoted here by $f_k$ for the $k$th dipole:

$$f_k = \left(\mathbf{a}_{3k-2}^T\mathbf{a}_{3k-2} + \mathbf{a}_{3k-1}^T\mathbf{a}_{3k-1} + \mathbf{a}_{3k}^T\mathbf{a}_{3k}\right)^{-p} \tag{11}$$

where $\mathbf{a}_i$ is the $i$th column of **A** and $p$ is a tunable depth weighting parameter. With this choice, the a priori variances of deeper sources will be larger than those of superficial ones. If Eq. (2) is interpreted to be a minimizer of a cost function composed of a weighted least-squares error and a penalty term which is a weighted norm of the currents (Liu et al., 2002), depth weighting amounts to assigning more penalty to the superficial currents. The larger the $p$, the more weighting there is; $p = 0$ corresponds to no depth weighting.

Previous studies suggest that use of $p = 0.5$ is suitable to improve the localization precision of MNE (Fuchs et al., 1999). However, this claim has not been validated in realistic brain models. We hypothesize that the optimal depth weighting depends on several factors, including local anatomy features, inter-subject variability, the inverse operator (i.e., with/without noise normalization), regularization parameter, and the decimation of source space. In the following section, we describe the process for performing parametric and quantitative analysis on a shift metric based on different values of the depth weighting parameter in order to provide the optimal depth weighting for accurate MEG localization using MNE.

### *Localization error metrics*

We employ two metrics to quantify spatial mis-localization. The depth shift ($S_{\mathrm{depth}}$) is the projected distance between the source dipole and the center of mass of the estimated source distribution in the direction from the source dipole to the closest point on the inner

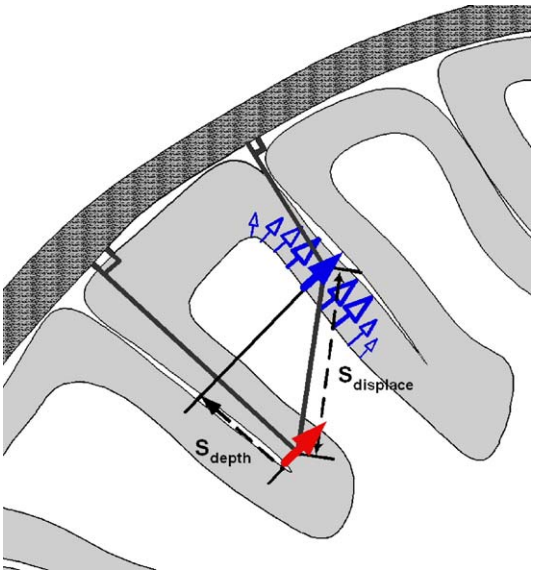


Fig. 1. The definition of metrics for quantifying mis-localization in the distributed MEG inverse solution. The red arrow indicates the site of the actual source. Blue arrows indicate the locations and magnitudes of the source estimates, and the solid blue arrow indicates the location of their center of mass. $S_{\mathrm{depth}}$ and $S_{\mathrm{displace}}$ represent the errors in depth and overall location, respectively, of the estimated source distribution. (For interpretation of the references to colour in this figure legend, the reader is referred to the web version of this article.)

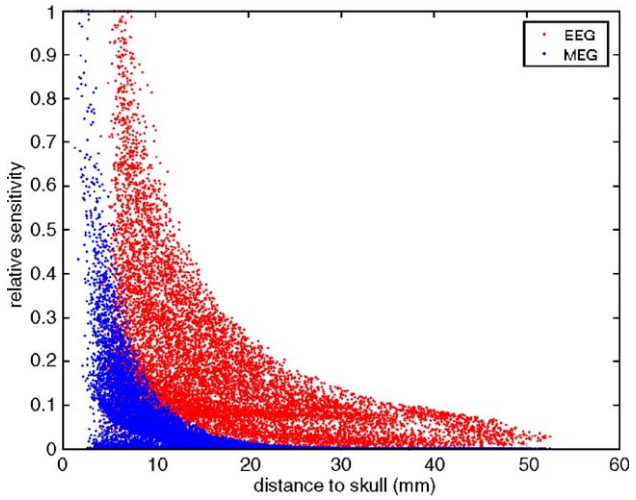


Fig. 2. The magnitude of the MEG (blue) and EEG (red) lead field as a function of distance to the skull. The values have been normalized by the maximum magnitude of the lead field within the source space. (For interpretation of the references to colour in this figure legend, the reader is referred to the web version of this article.)

skull surface. The displacement shift ($S_{\text{displace}}$) denotes the distance between the source dipole and the center of mass of the estimated source distribution. Fig. 1 is a schematic diagram illustrating the definition of these two metrics.

The rationale for using the center of mass in distributed current estimates is the spatially blurred nature of source localization. To avoid influence from the weak insignificant dipole estimates, we used only dipoles with amplitudes $|x(k)|$ exceeding 50% of the maximum amplitude. The center of mass was calculated as

$$\vec{r}_{cm} = \frac{\sum_k \vec{r}(k)|x(k)|}{\sum_k |x(k)|}, k \in \{X_{50\%}\}, \tag{12}$$

where $\{X_{50\%}\}$ indicates the collections of all dipoles with amplitudes exceeded 50% of the maximum amplitude, $\vec{r}_{(k)}$ is the source location indexed by $k$, and $\vec{r}_{cm}$ is the center of the mass.

We evaluated the effect of depth weighting by examining the MNE at each source location at different SNRs. The definition of SNR here is the ratio between the instantaneous power of the ideal MEG sensor measurements over that of the MEG sensor noises. In our experience, this SNR ranges from 4 to 100 in typical evoked-response MEG studies with 50–200 averages. We chose SNR = 25

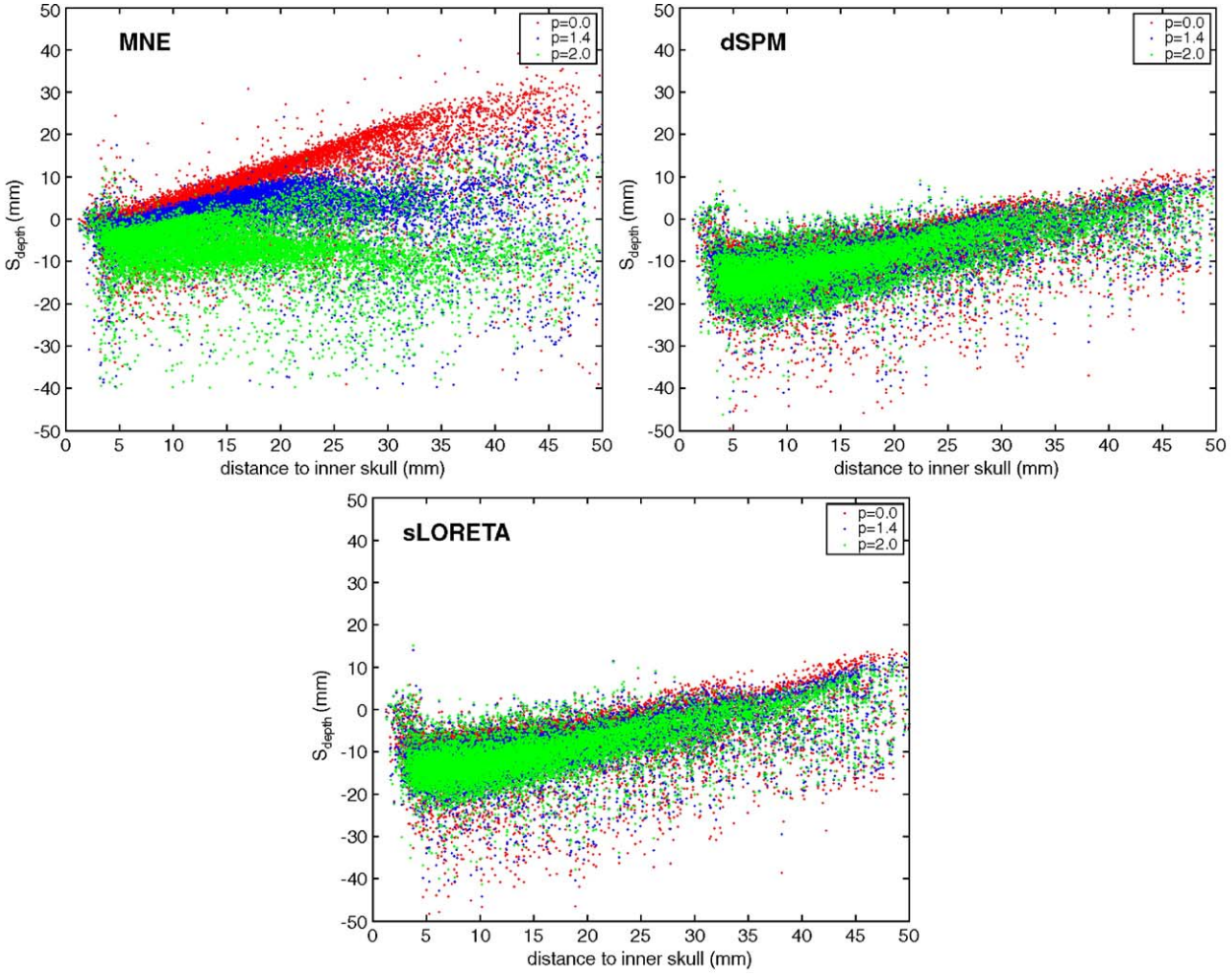


Fig. 3. The scatter plots of $S_{\text{depth}}$ versus the distance to the inner skull for $p$ = 0.0, 0.7 and 1.0 for MNE, dSPM, and sLORETA. With free dipole orientation, we found that MNE with $p$ = 0.7 gave the smallest average $S_{\text{depth}}$ and $S_{\text{displace}}$. Both dSPM and sLORETA show little variation of $S_{\text{depth}}$ at different depth weightings.

in the first simulation, and subsequently we varied SNR between 1 and 100.

We varied $p$ parametrically from 0.0 to 1.0 in steps of 0.05 for both EEG and MEG data. At each value of $p$, we evaluated the MNE (Eqs. (2) and (3)) and the noise-normalized MNE (dSPM and sLORETA, Eqs. (8) and (9)). For each source dipole on the cortical surface, we computed the forward solution and the corresponding inverse estimate, which is commonly called the point-spread function (PSF). For each inverse estimate, we computed the center of mass of the distribution and the error metrics described above.

Additionally, we use receiver operating characteristic (ROC) analysis to quantify the sensitivity and specificity of source localization with various depth weightings. The true-positive rate (TPR) of the detection was either 0 or 1 since we used single ECD in the simulation. The false-positive rate (FPR) at a given threshold was calculated as the fraction of the active cortical dipole sources, excluding the actual simulated active dipole source, over all cortical dipole sources. By varying the threshold, an ROC curve was obtained for each source dipole. We used the area under the ROC curve to quantify the detection power. The averaged ROC areas across all source dipoles thus provided the average detection assessment for a specific depth weighting.

### *Anatomical information from high-resolution MRI*

Anatomical MRI data were obtained from three subjects with a high-resolution T1-weighted 3D sequence (TR/TE/flip = 2530 ms/3.49 ms/7°, partition thickness = 1.33 mm, matrix = 256 × 256, 128 partitions, field of view = 21 cm × 21 cm) in a 1.5-T MRI scanner (SIEMENS Medical Solutions, Erlangen, Germany). The geometry of the gray–white matter surface was derived with an automatic segmentation algorithm to yield a triangulated model with approximately 340,000 vertices (Dale et al., 1999; Fischl et al., 1999, 2001). The source space was obtained by decimating the original triangulation to a subset of vertices with an average of 5-mm, 7-mm or 10-mm distance between nearest dipoles. Cortical Patch Statistics (Lin et al., 2006) were calculated as described above to obtain average normal directions, their standard deviations, and approximate patch areas for each source point. The MEG and EEG forward models were calculated using a single-layer/3-layer boundary element model (BEM) (Hamalainen and Sarvas, 1989; Oostendorp and van Oosterom, 1989). For this, we used segmentation algorithms to extract the inner surface of the skull and created the corresponding triangulation with approximately 1400 triangles.

### *Auditory and somatosensory MEG experiments*

We also used data from an auditory and a somatosensory MEG experiment to test our methods in realistic situations. The experiments were conducted with healthy subjects with the approval of the institutional IRB. Prior to the experiments, an informed consent was obtained from the subjects. In the auditory experiment, the stimuli were 60-ms wide-band noise bursts (2 kHz central frequency with 4 kHz bandwidth, 70 ms duration) presented binaurally. A 306-channel MEG system with 70-channel EEG (VectorView, Elekta-Neuromag, Helsinki, Finland) was used to record the neuromagnetic responses and EEG. The EEG electrodes were arranged to approximate the standard 20–20 layout. The measurement bandwidth was 0.1 to 172 Hz, and the data were digitized at 600 Hz; about 200 responses were averaged. In the somatosensory study, the right median nerve was stimulated at the wrist with 0.2 ms constant-current pulses whose amplitude was

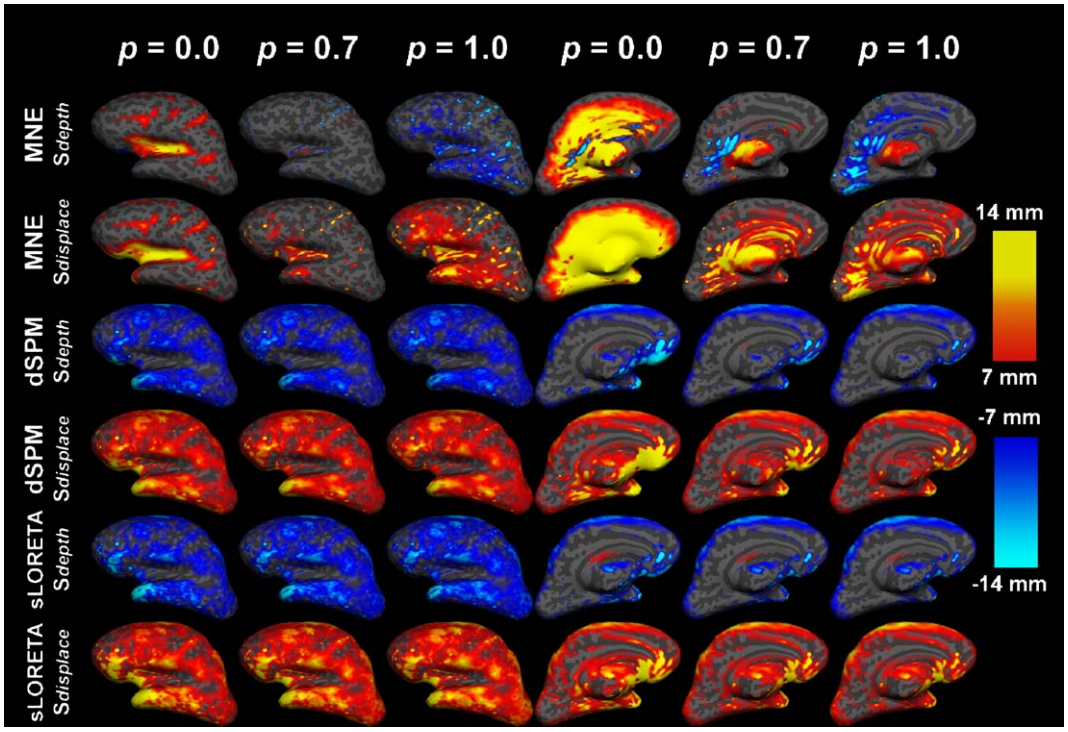


Fig. 4. The distribution of $S_{depth}$ and $S_{displace}$ in MNE, dSPM, and sLORETA inverse using different depth weighting parameters $p$ on the inflated cortex at the lateral and the medial views. In the figure, the light and dark gray indicate convex and concave parts of the cortex, respectively.

clearly above the motor threshold. The inter-stimuli interval between the pulses was 3 s. The measurement bandwidth was 0.03 to 250 Hz, and the data were digitized at 1004 Hz; about 100 responses were averaged.

## Results

### *MEG and EEG lead field magnitudes*

Fig. 2 illustrates the magnitude of EEG and MEG lead field as a function of the distance to the skull. The MEG lead field magnitude diminishes very fast as the distance from a dipole source to the skull increases. The observation motivates the use of depth weighting in MEG source localization. As seen from Fig. 2, the fall off of the EEG lead field is not as steep. These data imply that (1) both MEG and EEG may benefit from depth weighting and (2) the optimal depth weighting for MEG and EEG should be different.

### *Spatial distribution of localization error measures*

Scatter plots of $S_{depth}$ versus source distance from the inner surface of the skull for $p$ = 0.0, 0.7, and 1.0 are shown in Fig. 3. Without depth weighting, MNE showed a large $S_{depth}$ for deep sources. Using depth weighting with $p$ = 0.7 in MNE, $S_{depth}$ can be reduced uniformly at all depths, as shown by more horizontal distribution of the scatter plot. A larger value ($p$ = 1.0) caused $S_{depth}$ at all source locations to have negative values, indicating over-correction. Using linear regression, we found that intersects are 7.6 mm, 0.1 mm, and −7.4 mm, and slopes were −1.5, 0.1, and 1.3 with $p$ = 0.0, 0.7, and 1.0 respectively. The linear regression analysis with minimal absolute slope and intersect indicated improved $S_{depth}$ over all source locations. In dSPM and sLORETA, we found that $p$ = 0.0, 0.7, and 1.0 did not change the distribution of $S_{depth}$ significantly. The intersects and slopes of the regression in dSPM were −8.1 mm, −9.0 mm, −9.4 mm, and −2.0, −1.5, −1.2 with $p$ = 0.0, 0.7, and 1.0 respectively. For sLORETA, the intersects and slopes of the regression were −8.9 mm, −10.1 mm, −10.6 mm, and −0.2, 0.5, and 0.8 with $p$ = 0.0, 0.7, and 1.0, respectively.

Fig. 4 shows that, without depth weighting ($p$ = 0.0), MNE tended to bias the estimation of dipoles at insula and other sulcal regions as well as the medial surface of each hemisphere toward superficial locations, as shown by the prominent (>7 mm) $S_{depth}$ over these locations. Using noise normalization, we found that dipoles located at sulci or insula regions showed smaller $S_{depth}$, but, for superficial (gyral) regions, both dSPM and sLORETA inverse

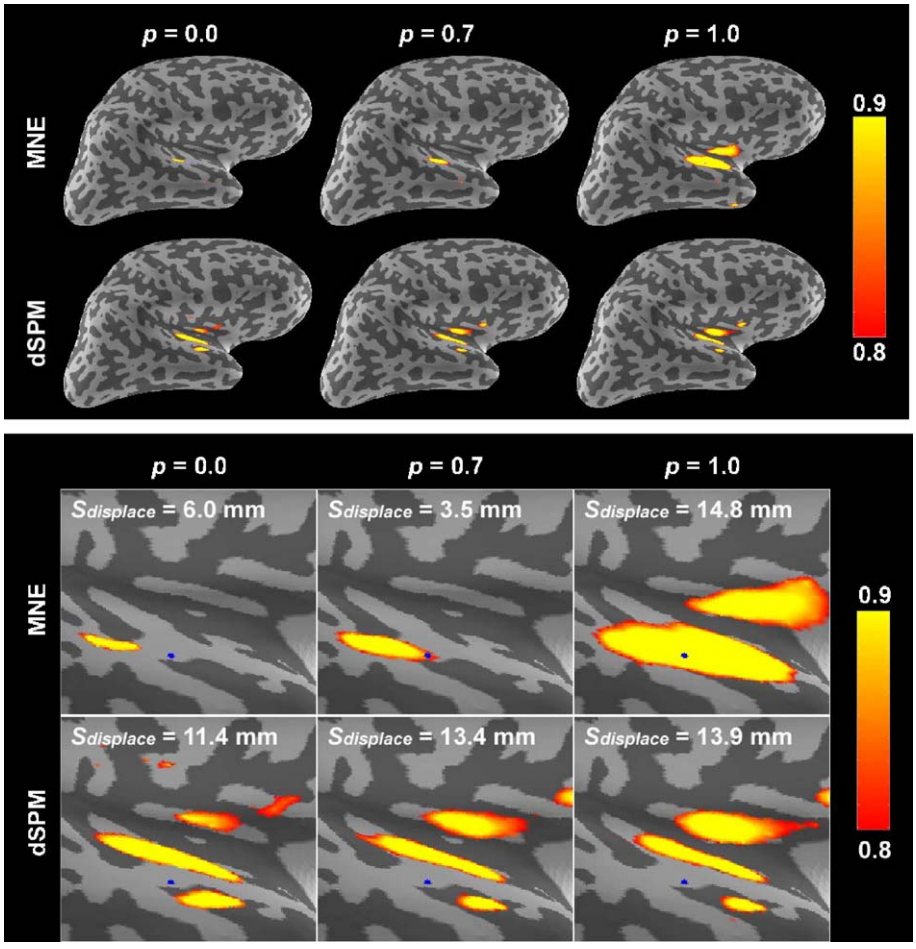


Fig. 5. The point-spread functions for a source (the blue dot) at the superior temporal gyrus (STG) for MNE and dSPM with different values of the depth weighting parameter $p$. Top panel is the view including whole cortex, and bottom panel is the magnified view at the temporal lobe. All point-spread functions are linearly scaled between 0 and 1 to illustrate their spatial distributions. The $S_{displace}$ between the center of the mass of MNE and dSPM and the dipole source at auditory cortex are indicated in each panel.

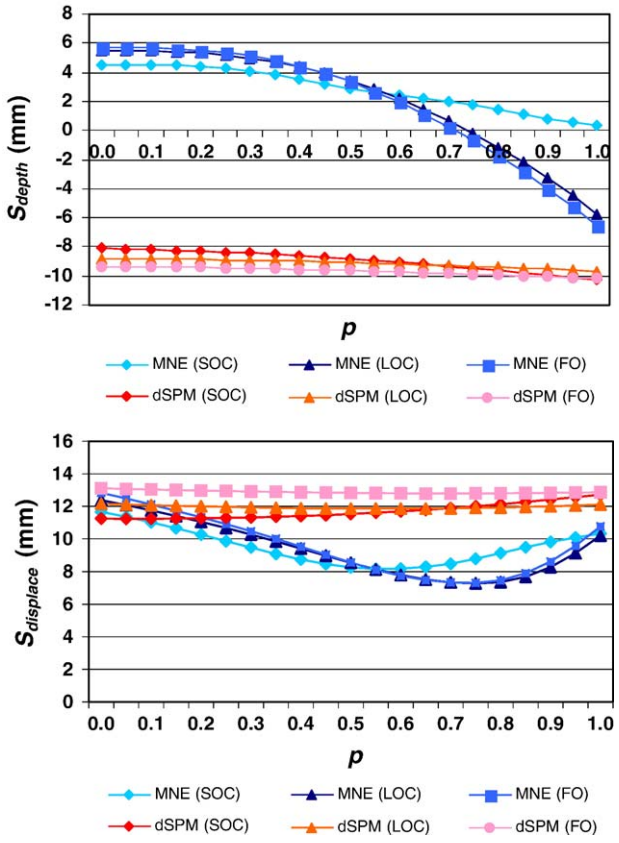


Fig. 6. Change of the average $S_{depth}$ and $S_{displace}$ over the cortex in MNE and dSPM as a function of the depth weighting parameter $p$ with free source orientations (FO), loose cortical orientation constraint (LOC), and strict cortical orientation constraint (SOC).

tended to over-bias the inverse toward deep dipole locations, as shown by the strong negative values of $S_{depth}$ in Fig. 3. dSPM and sLORETA showed similar spatial distribution of $S_{depth}$. Generally, MNE, dSPM, and sLORETA have substantial localization errors as assessed by $S_{displace}$. Nevertheless, dSPM tends to yield more homogeneous localization error than MNE, as reported in Dale et al. (2000). With $p = 0.7$, both $S_{depth}$ and $S_{displace}$ became smaller for the MNE. The improvement in the localization accuracy was evident in both lateral and medial aspects of the cortex. In contrast to MNE, dSPM and sLORETA showed little dependence on depth weighting. With $p = 1.0$, the MNE over-emphasized the depth of the superficial dipoles (the negative $S_{depth}$ in Fig. 1) and showed decreased localization accuracy (the positive $S_{displace}$ in Fig. 1). Again, dSPM and sLORETA showed only minor changes in both $S_{depth}$ and $S_{displace}$ compared to $p = 0.0$ and $p = 0.7$.

*Point-spread functions*

Fig. 5 shows the PSFs of MNE and dSPM inverse with $p = 0.0$, 0.7, and 1.0 for a dipole located at the superior temporal gyrus (STG) of the right hemisphere. To compare the spatial distribution at different depth weightings, all PSFs were linearly scaled between 0.0 and 1.0 to illustrate their spatial distribution. In MNE, without depth weighting ($p = 0.0$) shows bias of the source estimates toward the posterior parts of the superior temporal gyrus. Using $p = 0.7$, the distribution of the source estimates shifted anterior to include the STG dipole. Increasing $p$ to 1.0 over-corrected the depth and showed source estimates not only in STG but also in insula. dSPM point-spread functions have split distribution on both the medial part of STG and superior temporal sulcus (STS) in all cases. Note that depth weighting with $p = 0.7$ and 1.0 also led to the spurious point-spread function of dSPM inverse at insula. Inside the figure, we also showed the $S_{displace}$. MNE with $p = 0.7$ gave the minimal distance (3.5 mm).

*Orientation constraints*

In MNE, increasing $p$ decreased $S_{depth}$ for free orientation (FO), strict cortical orientation constraint (SOC), and loose cortical orientation constraint (LOC). In particular, $p = 0.75$ made $S_{depth}$ less than 2 mm using FO or LOC while $p > 0.8$ lead to negative $S_{depth}$, which indicates the over-correction of depth weighting. The SOC MNE showed monotonically decreased $S_{depth}$ as $p$ increased from 0.0 (4.5 mm) to 1.0 (0.4 mm). In dSPM inverse, the averaged $S_{depth}$ varied between −8.0 mm and −10.0 mm with $p = 0.0$ and 1.0 in all cortical orientation constraints. Assessing localization accuracy using $S_{displace}$, we found that in MNE $p = 0.75$ yielded minimal $S_{displace}$ of 7–8 mm for LOC and FO. MNE using SOC has minimal $S_{displace}$ with $p = 0.6$ (8 mm). Minimal $S_{displace}$ for LOC and FO MNEs were found with $p = 0.75$ (7 mm). dSPM inverse yielded approximately 12 mm $S_{displace}$ as $p$ varying between 0.0 and 1.0. Fig. 6 shows the plots of $S_{depth}$ and $S_{displace}$ in MNE and dSPM with varying $p$ between 0.0 and 1.0 in all cortical orientation constraints.

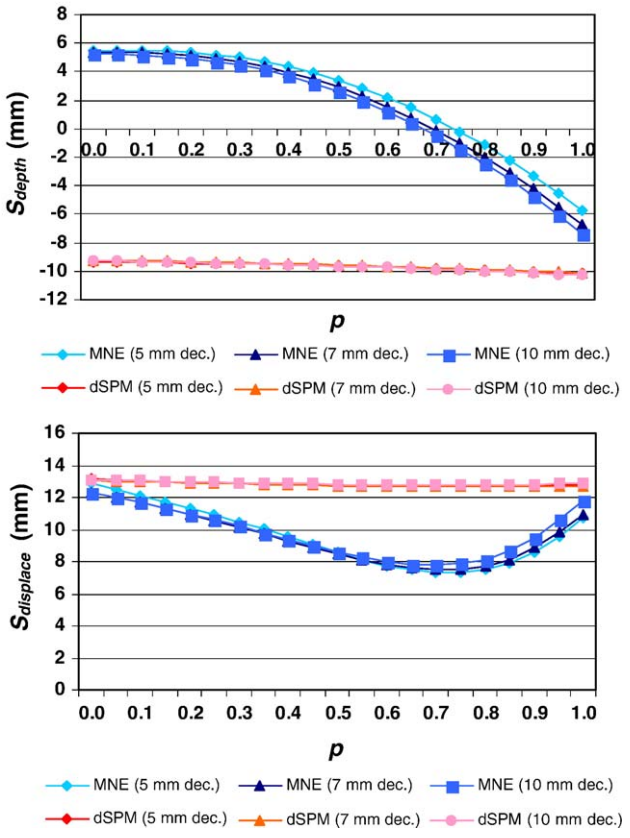


Fig. 7. Change of the average $S_{depth}$ and $S_{displace}$ over the cortex in MNE and dSPM as a function of the depth weighting parameter $p$ with 5-mm, 7-mm, and 10-mm source spacing.

*Source density*

Fig. 7 shows $S_{depth}$ and $S_{displace}$ for MNE and dSPM inverse using free orientation (FO) at different values of $p$ and 5-mm, 7-mm, or 10-mm spacing between sources. In general, both shift metrics in both MNE and dSPM demonstrate similar property in three different source densities. Increasing $p$ decreases $S_{depth}$ in MNE inverse with the minimum at $p = 0.7$ (7-mm and 10-mm spacing) or 0.75 (5-mm spacing). In MNE, $p \sim 0.7$ yielded minimal $S_{displace}$ (~8 mm) at three source space decimations. For dSPM, $S_{depth}$ or $S_{displace}$ do not change when $p$ varies between 0.0 and 1.0. $S_{depth}$ remains approximately −10 mm (over-correction of depth weighting) and remains approximately 13 mm for 5-mm, 7-mm, and 10-mm source space decimations.

*SNR and regularization parameter*

Changes to SNR and thus regularization parameter affect the optimal choice of $p$, as shown by Fig. 8. At low SNR (SNR = 1), $p = 0.65$ corresponds to the minimal $S_{depth}$ in MNE inverse. As SNR increases to 10 and then 100, the minimal $S_{depth}$ appears at $p = 0.75$. For the dSPM, the dependence of $S_{depth}$ on $p$ is, again, minimal: it remains approximately −9 mm (SNR = 10 or 100) or −12 mm (SNR = 1) at $p = 0.0$ and $p = 1.0$. Assessing localization precision using $S_{displace}$, we found that $p = 0.65$, 0.8, and 0.8 led to minimal $S_{displace}$ in MNE inverse as SNR = 1, 10, and 100, respectively. Low SNR (SNR = 1) corresponded to 15 mm $S_{displace}$. Higher SNR (SNR = 10 and 100) corresponds to 12 mm $S_{displace}$ as $p$ varies between 0.0 and 1.0.

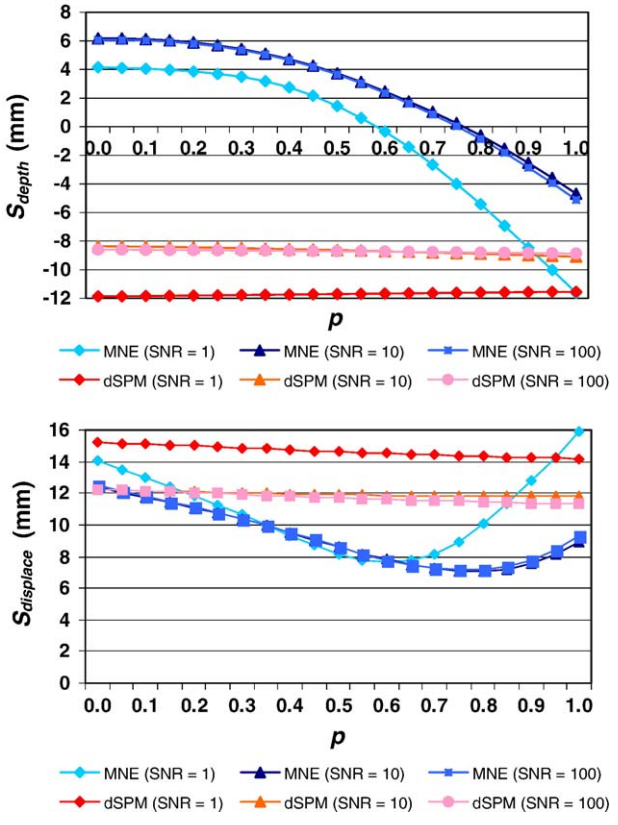


Fig. 8. Change of the average $S_{depth}$ and $S_{displace}$ over the cortex in MNE and dSPM as a function of $p$ as SNR varies between 1, 10, and 100.

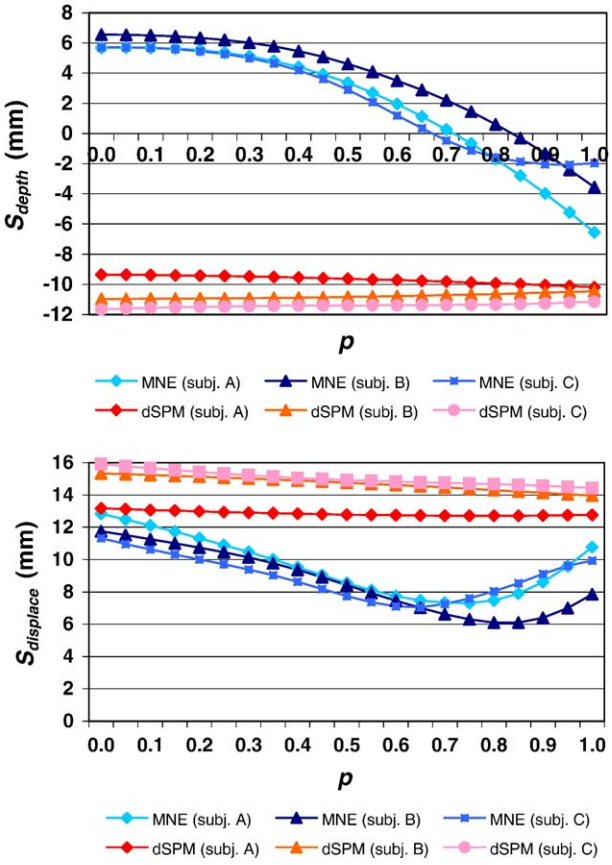


Fig. 9. Change of the average $S_{depth}$ and $S_{displace}$ over the cortex in MNE and dSPM as a function of the depth weighting parameter $p$ using free orientation in three different subjects.

*Inter-subject variability*

The dependency of $S_{depth}$ and $S_{displace}$ on $p$ across three different subjects for both MNE and dSPM with FO is shown in Fig. 9. Note that in general both shift metrics show similar patterns. For MNE, minimal $S_{depth}$ occurs at $p = 0.7$ and 0.85. And, minimal $S_{displace}$ occurs at $p = 0.65$ and 0.8. Again, dSPM remained insensitive to $p$. All subjects showed dSPM with −10 mm $S_{depth}$ and 14 mm $S_{displace}$. Averaged $S_{depth}$ and $S_{displace}$ for different subjects showed approximately 4-mm variability. In the subjects studied, the range of optimal $p$ is sufficiently small to justify the use of a fixed value, e.g., $p \sim 0.75$ for all subjects. However, especially for children with smaller and variable head sizes, it may be may be useful to establish an optimal $p$ by rerunning our simulations on individual subjects.

*Quantification of detection by true-positive rate (TPR)*

Fig. 10 shows the TPR at different depth weightings. For MNE, we found that TPR varied at different $p$. Increasing $p$ from 0 increased TPR for FO, LOC, and SOC MNE inverse. The maximal TPR was found with $p = 0.55–0.75$, depending on the orientation constraint used. This result matched the shift metrics reported in previous sections. For dSPM, we found that varying $p$ did not make significant change on TPR. The TPRs remained similar for FO, LOC, and SOC dSPM respectively. This observation also matched to the quantifica-

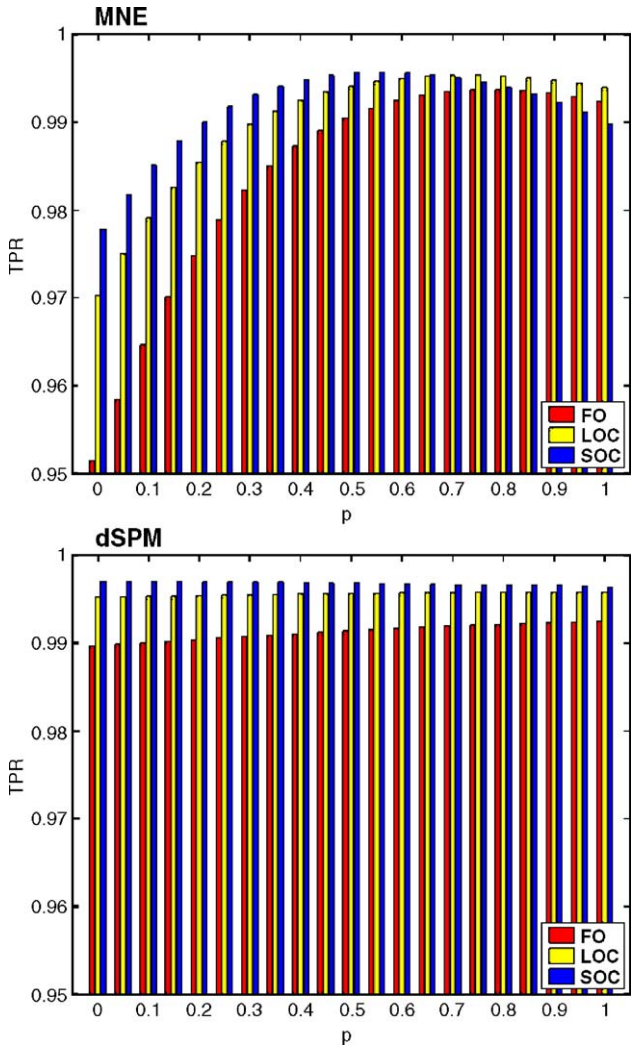


Fig. 10. True-positive-rate (TPR) of detection by MNE and dSPM as a function of the depth weighting parameter $p$ using free orientation.

tion by the shift metrics about dSPM's insensitivity to depth weighting.

*Depth weighting for EEG data*

Fig. 11 shows the dependency of $S_{\text{depth}}$ and $S_{\text{displace}}$ on $p$ for both MNE and dSPM with FO in EEG source localization. Note that the range of $p$ is different from MEG source localization: we varied $p$ in a wider range from 0.0 to 5.0 to reflect smoother power decay for deeper sources in EEG lead fields. A minimal $S_{\text{depth}}$ was found in EEG MNE at $p = 5.0$, while EEG dSPM showed biases toward deep source locations with all values of $p$ between 0.0 and 5.0. The minimal $S_{\text{displace}}$ occurred with $p = 2.0$, corresponding to 12.5 mm, while dSPM generated ranging between 24 and 26 mm at all $p$ between 0.0 and 5.0.

*Auditory and somatosensory experiments*

Fig. 12 shows the spatial distribution of MNE/dSPM inverse at 90 ms after the auditory stimulus. Without depth weighting, MNE inverse showed strong activation at both superior temporal gyrus (STG) and the inferior part of the central sulcus. At $p = 0.75$, MNE estimates major activation at STG and minor activation in insula. The activation pattern also moved anteriorly and medially along STG. At $p = 1.0$, strong activation around the insula was seen with minor activation at medial part of STG.

The MNE localization results on the somatosensory data and the related anatomical labels. Without depth weighting ($p = 0.0$), dominant activation was estimated at the post-central gyrus. With $p = 0.75$, the similar locus at post-central gyrus was estimated as well, along with additional estimated activation at central sulcus and pre-central gyrus. In real folded brain, these foci are actually next to each other. With $p = 1.0$, the spatial distribution of MNE is similar to the result with $p = 0.75$ with more focal estimated around central sulcus. Thus, this leads to the reduced MNE strength at other dipole locations as we normalized the inverse between 0 and 1.

## Discussion

This study focuses on compensating for the bias toward superficial sources in distributed $\ell_2$ minimum-norm estimates (MNE). Since the neuromagnetic inverse problem is ill-posed, MNE is just one approach to estimate the cortical current distribution among many other alternatives, such as dipole fitting and distributed source modeling with different priors (Hamalainen et al., 1993). Optimization of linear inverse operator was previously investigated by tuning the resolution kernel (Grave de Peralta Menendez et al., 1998; Grave de Peralta-Menendez and Gonzalez-Andino, 1998). The bias toward superficial is also present in $\ell_1$ minimum-norm estimates (Matsuura and Okabe,

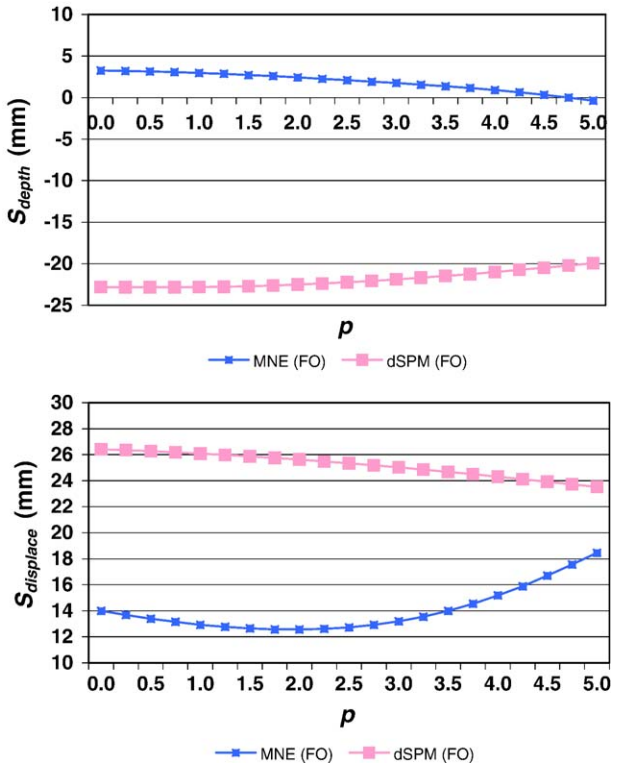


Fig. 11. Change of the average $S_{\text{depth}}$ and $S_{\text{displace}}$ over the cortex in MNE and dSPM as a function of the depth weighting parameter $p$ using free orientation in 70-channel EEG data.

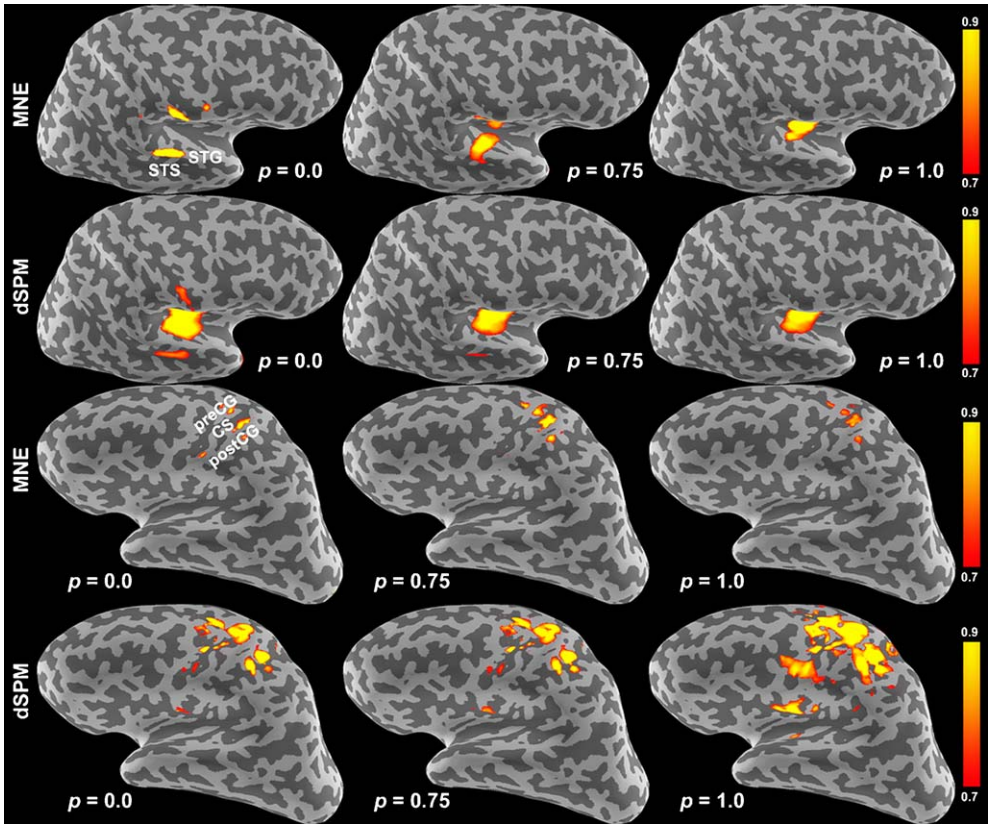


Fig. 12. The anatomical labels and the MNE inverse of the auditory data (top two rows) and somatosensory data (bottom two rows). MEG data as a function of the depth weighting parameter $p$. All inverse solutions were scaled linearly between 0 and 1 to illustrate the spatial distributions of the estimates. STG: superior temporal gyrus, STS: superior temporal sulcus, CS: central sulcus, preCG: pre-central gyrus, postCG: post-central gyrus.

1995), and the importance of depth weighting in this case has been shown previously (Uutela et al., 1999). In this study, we parametrically varied different model parameters in MNE, including cortical orientation constraints, SNR, and source space density, to demonstrate the improved localization accuracy of MNE with appropriate depth weighting.

Our results show that using $p = 0.7–0.8$ in general yields most accurate localization accuracy, as quantified by our shift metrics. Our value of $p$ is different from the one reported before (Fuchs et al., 1999), where $p = 0.5$ was suggested. In the data presented here, we found that the previously reported $p = 0.5$ is insufficient to correct the bias toward superficial sources. Our shift metrics are closely related to the concept of the point-spread function, which emerges from the resolution matrix (Pascual-Marqui, 2002). In fact, the columns of the resolution matrix are the point-spread functions for each of the sources of interest. In an ideal case, the resolution matrix should be an identity matrix corresponding to zero shift metrics.

The optimal depth weighting was calculated by assuming that sources of the neuromagnetic fields are focal. This assumption is the basis of the dipole modeling approach (Hamalainen et al., 1993; Mosher et al., 1992). Such focal sources have been observed in median nerve stimulation experiments (Hari et al., 1993) and epileptic spike generation (Ossadtchi et al., 2004). However, it has been also reported that cortical activation may be more diffuse, as suggested by fMRI studies showing distributed activation of brain during complex cognitive tasks (Dale and Halgren, 2001). In our search for the optimal depth weighting parameter, we aimed at minimizing location shifts for each individual source dipole. Thus, the proposed depth weighting parameter can work well if the recorded MEG data are generated by focal sources. On the other hand, cautions must be taken if it is believed that the recorded MEG signals are generated by more diffuse activity.

Mathematically, the calculation of the depth weighting parameter depends on the gain matrix (Eq. (11)). Thus, all factors that change the gain matrix may affect the optimal choice of the depth weighting parameter. Such factors include the spatial density of sources and cortical orientation constraints. For different SNRs, the balance between the anatomically determined lead field and functionally determined noise covariance is changed. We observed the changes of shift metrics in this study as these factors were varied parametrically. Fortunately, the optimal depth weighting parameter does not change dramatically as a function of source density, orientation constraints, or SNR: $p = 0.75$ in general leads to improved performance in MNE inverse.

We found that dSPM and sLORETA generated similar shift metrics, as shown in Figs. 3 and 4. It has been previously shown that dSPM alleviates the bias toward superficial sources (Dale et al., 2000). However, our data clearly show that dSPM in general overestimates the depth. When we increased the depth weighting parameter, the depth bias in MNE became smaller and the localization thus more accurate. In contrast, the dSPM and sLORETA inverses do not change significantly as a function of the depth weighting parameter. This characteristic is independent of the orientation constraint employed, source space density, and

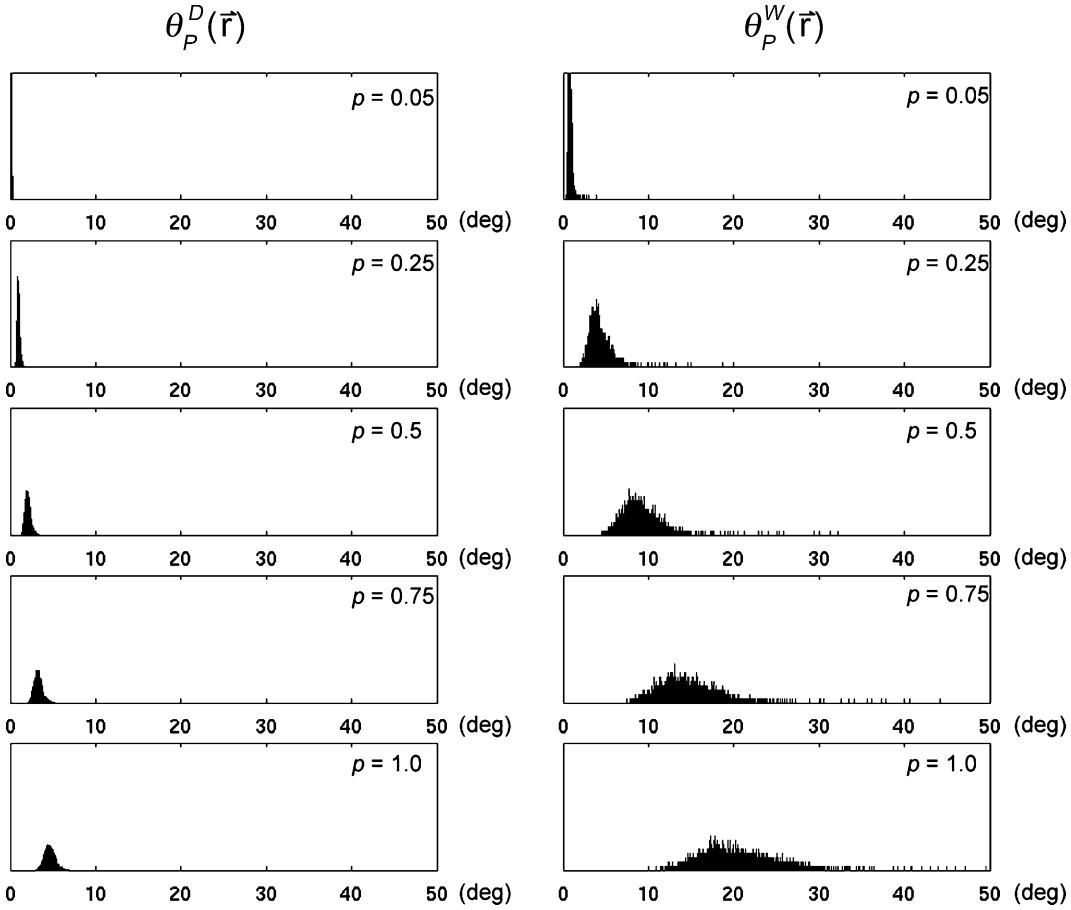


Fig. 13. The histogram of the defined "data covariance angle" and "inverse operator angle" at different depth weightings.

the subject. One explanation to this is that, in Eqs. (8) and (9), the dSPM can be interpreted as the estimated SNR of the sources. Since the same MNE inverse operator is employed in calculating both the signal and noise, any chances in it cancel out when the ratio of the two is computed. A similar effect was also reported in our recent study of human cortical oscillations using MEG data (Lin et al., 2004). In that case, we found that the fMRI priors do not change the dSPM inverse solution considerably, obviously due to the cancellation occurring in Eqs. (8) and (9). The insensitivity of dSPM/sLORETA to depth weighting is also evident from the expression of the inverse operator in Eq. (3). Each row of the first term ($\mathbf{R}\tilde{\mathbf{A}}^T$) is proportional to the corresponding element of the source covariance matrix, whereas the second term involving the product $\tilde{\mathbf{A}}\mathbf{R}\tilde{\mathbf{A}}^T$ is only weakly affected by the changes in the individual elements of $\mathbf{R}$.

To quantify this argument, we define the data covariance angle $\theta_P^d(\vec{r})$ with

$$\mathbf{d}_p(\vec{r}) = \left(\tilde{\mathbf{A}}\mathbf{R}_p\tilde{\mathbf{A}}^T + \lambda\mathbf{I}\right)^{-1}\tilde{\mathbf{b}}(\vec{r})$$

$$\theta_p^d(\vec{r}) = \arccos\left(\mathbf{d}_0^T\mathbf{d}_p/\left(|\mathbf{d}_0||\mathbf{d}_p|\right)\right)$$

where $\mathbf{R}_P$ is the source covariance matrix with depth weighting correction of order $p$ and $\tilde{b}(\vec{r})$ is the whitened field of a dipole, oriented normal to the cortical surface, at location $(\vec{r})$. Similarly, we define the *inverse operator angle*$(\vec{r})$ with

$$\mathbf{w}_p(\vec{r}) = \mathbf{R}_p\tilde{\mathbf{A}}^T\mathbf{d}_p(\vec{r})$$

$$\theta_p^w(\vec{r}) = \arccos\left(\mathbf{w}_0^T\mathbf{w}_p/\left(|\mathbf{w}_0||\mathbf{w}_p|\right)\right).$$

Fig. 13 shows the histograms of $\theta_P^d(\vec{r})$ and $\theta_P^w(\vec{r})$ at different depth weighting parameters $p$ across the whole source space. We found that $\theta_P^d(\vec{r})$ were distributed 0 and 8° at all source locations with similar histogram width at all depth weightings. In contrast, the distribution of $\theta_P^w(\vec{r})$ is wider than that of $\theta_P^d(\vec{r})$ and the mean increases to up to 40 degrees as $p$ is increased. This indicates that the major contribution in depth weighting comes from the $\mathbf{R}\tilde{\mathbf{A}}^T$ term in the inverse operator.

Another popular MEG source estimation approach is the minimum-variance beamformer (Van Veen et al., 1997). Recently, it has been shown that both the MNE and beamformer can be cast into an equivalent form (Mosher et al., 2003). In MNE, the data covariance matrix $\mathbf{D} = \mathbf{ARA}^T/\lambda^2 + \mathbf{C}$ is postulated by using an estimate of $\mathbf{C}$ and $\mathbf{R}$ based on the selected source priors. In the beamformer approach, $\mathbf{D}$ is actually estimated from the data. As shown by Mosher, the beamformer assumes the form of a MNE inverse if the source covariance is $\mathbf{R} = (\mathbf{A}^T\mathbf{D}^{-1}\mathbf{A}^{-1})$, where $\mathbf{D}$ is the estimated data covariance matrix. Thus, the beamformer implicitly incorporates depth weighting by calculating the weighted norm of the columns of $\mathbf{A}$. This explains why beamformer in general shows less bias toward superficial sources than MNE without depth

weighting. The obvious caveat of the equivalence between the MNE and beamformer obviously is that for MNE it is not guaranteed that the choice of **R** based on priors would give rise to the actual observed data covariance matrix nor that for the beamformer the implicit choice of $\mathbf{R} = (\mathbf{A}^{\mathbf{T}}\ \mathbf{D}^{-1}\mathbf{A}^{-1})$ would be the true **R** giving rise to actually observed data covariance matrix.

Our somatosensory and auditory data illustrate the benefit of depth weighting in MNE. Using $p = 0.75$, we found that depth weighting does not overestimate depth of the sulcal sources in the somatosensory experiment, and it provides better localization of activities to Heschl's gyrus in the auditory experiment. These data as well as our simulations clearly demonstrate that depth weighting is a robust approach to reduce the source location bias.

## Acknowledgments

We appreciate the comments from Dr. Jyrki P. Ahveninen on the manuscript. This work was supported by National Institutes of Health Grants R01 HD040712, R01 NS037462, P41 RR14075, the Mental Illness and Neuroscience Discovery Institute (MIND).

## References

Dale, A.M., Halgren, E., 2001. Spatiotemporal mapping of brain activity by integration of multiple imaging modalities. Curr. Opin. Neurobiol. 11, 202–208.

Dale, A., Sereno, M., 1993. Improved localization of cortical activity by combining EEG and MEG with MRI cortical surface reconstruction: a linear approach. J. Cogn. Neurosci. 5, 162–176.

Dale, A.M., Fischl, B., Sereno, M.I., 1999. Cortical surface-based analysis: I. Segmentation and surface reconstruction. NeuroImage 9, 179–194.

Dale, A.M., Liu, A.K., Fischl, B.R., Buckner, R.L., Belliveau, J.W., Lewine, J.D., Halgren, E., 2000. Dynamic statistical parametric mapping: combining fMRI and MEG for high-resolution imaging of cortical activity. Neuron 26, 55–67.

Fischl, B., Sereno, M.I., Dale, A.M., 1999. Cortical surface-based analysis. II: Inflation, flattening, and a surface-based coordinate system. NeuroImage 9, 195–207.

Fischl, B., Liu, A., Dale, A.M., 2001. Automated manifold surgery: constructing geometrically accurate and topologically correct models of the human cerebral cortex. IEEE Trans. Med. Imag. 20, 70–80.

Fuchs, M., Wagner, M., Kohler, T., Wischmann, H.A., 1999. Linear and nonlinear current density reconstructions. J. Clin. Neurophysiol. 16, 267–295.

Grave de Peralta-Menendez, R., Gonzalez-Andino, S.L., 1998. A critical analysis of linear inverse solutions to the neuroelectromagnetic inverse problem. IEEE Trans. Biomed. Eng. 45, 440–448.

Grave de Peralta Menendez, R., Hauk, O., Gonzalez Andino, S., Vogt, H., Michel, C., 1998. Linear inverse solutions with optimal resolution kernels applied to electromagnetic tomography. Hum. Brain Mapp. 5, 454–467.

Hamalainen, M., Ilmoniemi, R., 1984. Interpreting measured magnetic fields of the brain: estimates of current distributions. Technical Report, Helsinki University of Technology, TKK-F-A559.

Hamalainen, M.S., Sarvas, J., 1989. Realistic conductivity geometry model of the human head for interpretation of neuromagnetic data. IEEE Trans. Biomed. Eng. 36, 165–171.

Hamalainen, M., Hari, R., Ilmoniemi, R., Knuutila, J., Lounasmaa, O., 1993. Magnetoencephalography—Theory, instrumentation, and application to noninvasive studies of the working human brain. Rev. Modern Phys. 65, 413–497.

Hari, R., Karhu, J., Hamalainen, M., Knuutila, J., Salonen, O., Sams, M., Vilkman, V., 1993. Functional organization of the human first and second somatosensory cortices: a neuromagnetic study. Eur. J. Neurosci. 5, 724–734.

Heller, L., van Hulsteyn, D.B., 1992. Brain stimulation using electromagnetic sources: theoretical aspects. Biophys. J. 63, 129–138.

Helmholtz, H., 1853. Ueber einige Gesetze der Vertheilung elektrischer Strome in korperlichen Leitern, mit Anwendung auf die thierisch-elektrischen Versuche. Ann. Phys. Chem. 89, 211–233, 353–377.

Hillebrand, A., Barnes, G.R., 2002. A quantitative assessment of the sensitivity of whole-head MEG to activity in the adult human cortex. NeuroImage 16, 638–650.

Ioannides, A.A., Bolton, J.P., Clarke, C.J.S., 1990. Continuous probabilistic solutions to the biomagnetic inverse problem. Inverse Problems 6, 523–542.

Lin, F.-H., Belliveau, J.W., Dale, A.M., Hamalainen, M.S., 2003. Minimum-current estimates with a cortical orientation constraint. The 9th Annual Meeting of the Organization for Human Brain Mapping, p. s45.

Lin, F.-H., Witzel, T., Hamalainen, M.S., Dale, A.M., Belliveau, J.W., Stufflebeam, S.M., 2004. Spectral spatiotemporal imaging of cortical oscillations and interactions in the human brain. Neuroimage 23, 582–595.

Lin, F.H., Belliveau, J.W., Dale, A.M., Hamalainen, M.S., 2006. Distributed current estimates using cortical orientation constraints. Hum. Brain. Mapp. 27, 1–13.

Liu, A.K., Dale, A.M., Belliveau, J.W., 2002. Monte Carlo simulation studies of EEG and MEG localization accuracy. Hum. Brain Mapp. 16, 47–62.

Matsuura, K., Okabe, Y., 1995. Selective minimum-norm solution of the biomagnetic inverse problem. IEEE Trans. Biomed. Eng. 42, 608–615.

Mosher, J.C., Lewis, P.S., Leahy, R.M., 1992. Multiple dipole modeling and localization from spatio-temporal MEG data. IEEE Trans Biomed. Eng. 39, 541–557.

Mosher, J.C., Baillet, S., Leahy, R.M., 2003. Equivalence of linear approaches in biomagnetic inverse solutions. 2003 IEEE Workshop Stat. Signal Process, 294–297.

Oostendorp, T.F., van Oosterom, A., 1989. Source parameter estimation in inhomogeneous volume conductors of arbitrary shape. IEEE Trans. Biomed. Eng. 36, 382–391.

Ossadtchi, A., Baillet, S., Mosher, J.C., Thyerlei, D., Sutherling, W., Leahy, R.M., 2004. Automated interictal spike detection and source localization in magnetoencephalography using independent components analysis and spatio-temporal clustering. Clin. Neurophysiol. 115, 508–522.

Pascual-Marqui, R.D., 2002. Standardized low-resolution brain electromagnetic tomography (sLORETA): technical details. Methods Find. Exp. Clin. Pharmacol. 24 (Suppl D.), 5–12.

Phillips, C., Rugg, M.D., Friston, K.J., 2002. Anatomically informed basis functions for EEG source localization: combining functional and anatomical constraints. NeuroImage 16, 678–695.

Tarantola, A., 1987. Inverse problem theory: methods for data fitting and model parameter estimation, Elsevier; distributors for the United States and Canada Elsevier Science Pub. Co., Amsterdam; New York, New York, NY.

Uutela, K., Hamalainen, M., Somersalo, E., 1999. Visualization of magnetoencephalographic data using minimum current estimates. NeuroImage 10, 173–180.

Van Veen, B.D., van Drongelen, W., Yuchtman, M., Suzuki, A., 1997. Localization of brain electrical activity via linearly constrained minimum variance spatial filtering. IEEE Trans. Biomed. Eng. 44, 867–880.

Wang, J.Z., Williamson, S.J., Kaufman, L., 1992. Magnetic source images determined by a lead-field analysis: the unique minimum-norm least-squares estimation. IEEE Trans. Biomed. Eng. 39, 665–675.